Spin dynamics for wave packets in Rashba systems

Bailey C. Hsu* and Jean-François S. Van Huele†
Department of Physics and Astronomy, Brigham Young University, Provo, Utah 84602, USA
(Received 24 June 2009; revised manuscript received 2 November 2009; published 8 December 2009)

We explore spin dynamics for localized wave packets in Rashba systems using spin quantum propagators. We derive exact (one-dimensional) and approximate (two-dimensional) analytic expressions for the propagators and apply them to Gaussian wave packets to obtain localized solutions of systems manifesting Rashba interactions. We observe and describe the evolution of the wave packets. We identify characteristic structures in the wave-packet evolution and look for features with specific spintronics applications such as spin separation and spin accumulation. We discuss the relative importance of those features as a function of the Rashba coupling strength α and the width of the wave packet w. In particular, we find a trade off between spatial oscillation and global separation of the spin when varying α and w.

DOI: 10.1103/PhysRevB.80.235309 PACS number(s): 71.70.Ej, 73.21.Hb, 85.75.−d

I. INTRODUCTION

Spintronics is a promising technology where the focus is on manipulating the spin degree of freedom of electrons in addition to their charge.[1–4] Efficient spin injection, spin transport, and spin detection need to be achieved to insure the functionality of spintronics devices. Among the many areas of interest in spintronics, spin-orbit coupling (SOC) is an important mechanism to control spin dynamics without introducing an external magnetic field.[5] All spin-orbit coupled systems that have been proposed share one common characteristic: their Hamiltonians couple momentum and/or position operators to spin operators. These systems have been studied to exhibit various spin-dependent phenomena including spin-Hall effect,[6–8] quantum spin-Hall effect,[9] spin accumulation at the edge,[10] persistent spin-helix,[11,12] and *Zitterbewegung-like* motion for wave packets.[13,14] The presence of two or more incompatible (noncommuting) spin operators in the Hamiltonian adds a layer of dynamical complexity for electrons carrying specific spin components. Two widely discussed SOC contributions are the Rashba and the Dresselhaus effects.[15–17] The Rashba effect is the signature of structure inversion asymmetry present in quantum wells while the Dresselhaus effect is the signature of bulk inversion asymmetry present in zinc-blende structures lacking inversion symmetry. The spin degree of freedom in the Rashba system has also been proposed to construct a Rashba adder and more general functions of a spin logic circuits.[18–20]

Several treatments have been applied to analyze the spin dynamics inside Rashba systems: Heisenberg picture method,[13] linear-response theory,[21] fixed energy Green function,[22–24] direct numerical integration,[25,26] and density-matrix approach.[27] In this contribution we develop the quantum-mechanical spin propagator method from the Schrödinger equation for Rashba SOC interaction in one-dimensional (1D) and two-dimensional (2D) condensed-matter systems. The advantage of calculating the propagator separately is that it can be applied to any initial state. Rather than dealing with plane waves we choose to study localized solutions, in particular, spin-polarized Gaussian wave packets, which are interesting in their own right. For example, phenomena such as Zitterbewegung are known to be transient for wave packets[28] including in condensed-matter systems.[29,30] Results from Gaussian wave-packet dynamics have been obtained previously[13,26] and we mention how our results obtained using the propagator in closed forms compare with them. We also study the dependence of the results on the Rashba coupling strength (in the Hamiltonian) and on the localization (width of the wave packet). We display plots of the polarization at specific times while controlling these two parameters.

The paper is organized as follows: in Sec. II, we briefly introduce two analytic propagator construction methods. We give the exact analytic quantum propagators which we derived for the 1D Rashba system with harmonic confining potential. We also give approximate analytic quantum propagators based on the Trotter formula for the 2D Rashba system. In Sec. III, we first construct the spin densities in the 1D Rashba system by applying the specific analytic propagator to an initial Gaussian wave packet in space and polarized along specific directions and we identify four characteristic features. We then generate wave-packet evolutions numerically and highlight four new features of the spin densities in the 2D Rashba system. In the 2D case, in addition to changing the overall width of the wave packet, we also consider the effect of uneven widths in two dimensions on the result. In Sec. IV we discuss our results and make a qualitative comparison between different cases and by connecting to current spintronics research.

II. PROPAGATOR CONSTRUCTION

The propagator $K(x,x_0;t-t')$ gives the conditional transition amplitude between two position eigenstate vectors $|x\rangle$ and $|x_0\rangle$ over a time interval $t-t'$ such that $K(x,x_0;t-t')=\langle x|U(t-t')|x_0\rangle$, where $U(t-t')$ is the time-evolution operator.[31] Without loss of generality we set $t'=0$ in this paper. Because the Hamiltonians we consider involve spin operators, the propagators have a 2×2 matrix representation for spin-1/2 particles. We now proceed to construct analytic expressions of propagators using two different analytic methods applied to the 1D and 2D Rashba systems, respectively.

The Hamiltonian for the confined 1D Rashba system is

$$\mathcal{H} = \frac{p_x^2}{2m} - \frac{\alpha}{\hbar}\sigma_y p_x + \frac{1}{2}m\omega^2 x^2, \tag{1}$$

where α is the experimentally controlled Rashba coupling strength, σ_y is the Pauli spin operator, and ω is the confinement strength. We have obtained exact analytic expressions for the propagator for the confined ($\omega \neq 0$) and the unconfined ($\omega=0$) case using an analytic method based on the manipulation of noncommuting operators in exponentials.[32,33] After lengthy but straightforward calculations one obtains the 1D confined Rashba propagator $K_{1D}^c(x,x_0;t)$

$$K_{1D}^c = \sqrt{\frac{m\omega}{2\pi i\hbar \sin \omega t}}\exp\left\{\frac{im}{2\hbar}\left[(x^2+x_0^2)\omega\cot\omega t - 2xx_0\omega \csc \omega t - \frac{2\alpha\sigma_y}{\hbar}(x-x_0) + \frac{\alpha^2}{\hbar^2}t\right]\right\}. \tag{2}$$

By setting $\omega=0$ in the Hamiltonian in Eq. (1), we also derive the 1D unconfined Rashba propagator $K_{1D}^u(x,x_0;t)$

$$K_{1D}^u = \sqrt{\frac{m}{2\pi i\hbar t}}\exp\left[-\frac{m\left(x-x_0+\frac{\alpha\sigma_y t}{\hbar}\right)^2}{2i\hbar t}\right]. \tag{3}$$

We note that the expression for K_{1D}^u is also recovered in the unconfined limit $\omega\to 0$ in the propagator in Eq. (2). It can be checked that the corresponding propagators for vanishing Rashba term ($\alpha=0$) K_{1D}^c in Eq. (2) and K_{1D}^u in Eq. (3) reduce to the 1D simple harmonic-oscillator propagator and the 1D free-particle propagator, respectively.[31]

The Hamiltonian for the 2D Rashba system with parabolic confinement in x and unconfined in y is

$$\mathcal{H} = \frac{p_x^2+p_y^2}{2m} + \frac{\alpha}{\hbar}(p_y\sigma_x - p_x\sigma_y) + \frac{1}{2}m\omega^2 x^2. \tag{4}$$

The presence of two noncommuting Pauli matrices in the Hamiltonian makes it more challenging to obtain the propagator in closed form.[27] Therefore we construct approximate analytic expressions for the propagator in the confined ($\omega \neq 0$) and the unconfined ($\omega=0$) case using an analytic method based on the Trotter formula generalized to spin systems.[34] The Trotter formula for two noncommuting operators a and b, exact to $\mathcal{O}(\tau^3)$, gives

$$e^{-\tau(a+b)} = e^{-\tau a/2}e^{-\tau b}e^{-\tau a/2} + \mathcal{O}(\tau^3). \tag{5}$$

By replacing a and b with the potential term V and the kinetic term T, respectively, in the time-evolution operator $U(t)=e^{-it(T+V)/\hbar}$ and by setting $\tau=it/\hbar$, the propagator K is obtained by projecting the time-evolution operator $U(t)$ on position eigenvectors

$$K = \langle x|U(t)|x_0\rangle \approx \langle x|e^{-itV/2\hbar}e^{-itT/\hbar}e^{-itV/2\hbar}|x_0\rangle. \tag{6}$$

A Trotter formula exact to $\mathcal{O}(\tau^5)$ can be used to give exact analytical result for the free particle and the linear potential problem. For the confined Rashba potential in Eq. (4), we evaluate the propagator correctly to order τ^3. In Eq. (4), noncommutativities appear both between position and momentum operators and between Pauli matrices. Instead of setting a and b equal to the potential and kinetic terms, respectively, we extract from Eq. (4) the parts for which the propagator can be found analytically [in analogy to Eq. (2) in the x direction and to Eq. (3) in the y direction] and set them equal to b, such that $b=\frac{\mathbf{p}^2}{2m}+\frac{\alpha}{\hbar}(p_y-p_x)\sigma_x+\frac{m\omega^2x^2}{2}$ and $\mathbf{p}^2=p_x^2+p_y^2$. The Trotter formula can now be applied with the remaining terms set equal to a, namely, $a=\frac{\alpha}{\hbar}p_x(\sigma_x-\sigma_y)$.

After some algebraic manipulations, the propagator $K_{2D}^c(x,x_0,y,y_0;t)$ is obtained for the 2D (semi)confined Rashba system

$$K_{2D}^c \approx \sqrt{\frac{\omega}{t\sin\omega t}}\frac{m}{2\pi i\hbar}\exp\left\{\frac{im}{2\hbar}\left[\left(x^2+x_0^2+\frac{\alpha^2t^2}{\hbar^2}\right)\times\omega\cot\omega t - \left(2xx_0+\frac{\alpha^2t^2}{\hbar^2}\right)\omega\csc\omega + \frac{\alpha^2t}{\hbar^2} + \omega(\cot\omega t+\csc\omega t)\frac{\alpha t}{\hbar}(\sigma_x-\sigma_y)(x-x_0) - \frac{2\alpha\sigma_x}{\hbar}(x-x_0) + \frac{\left(y-y_0+\frac{\alpha\sigma_x t}{\hbar}\right)^2}{t}\right]\right\}. \tag{7}$$

By setting $\omega=0$ in the Hamiltonian in Eq. (4), we derive the 2D unconfined Rashba propagator $K_{2D}^u(x,x_0;t)$

$$K_{2D}^u \approx \frac{m}{2\pi i\hbar t}\exp\left\{-\frac{m}{2i\hbar t}\left[\left(x-x_0+\frac{\alpha\sigma_y t}{\hbar}\right)^2 + \left(y-y_0-\frac{\alpha\sigma_x t}{\hbar}\right)^2\right]\right\}. \tag{8}$$

We can also recover the expression K_{2D}^u in the unconfined limit $\omega\to 0$ of the propagator in Eq. (7). The corresponding propagators for vanishing Rashba terms ($\alpha=0$) can be checked: K_{2D}^c in Eq. (7) and K_{2D}^u in Eq. (8) reduce to the 2D simple harmonic oscillator and 2D free-particle propagator, respectively.[31]

Once the propagator is obtained, we can obtain the wave-packet evolution $\psi(x,t)$ by applying it to an initial wave packet $\psi(x_0,0)$

$$\psi(x,t) = \int_{-\infty}^{\infty} K(x,x_0;t)\psi(x_0,0)dx_0. \tag{9}$$

In this work we choose $\psi(x_0,0)$ to be a spinor with Gaussian distribution in space centered at $x_0=0$ and with width w, such that $\psi(x_0,0)=\frac{1}{\sqrt{\pi w}}\exp(-x_0^2/2w^2)(\chi|\uparrow\rangle+\xi|\downarrow\rangle)$, where $|\uparrow\rangle$ and $|\downarrow\rangle$ are up-in-z and down-in-z spin states with constant coefficients χ and ξ chosen to satisfy $|\chi|^2+|\psi|^2=1$. Because of the linearity of the Schrödinger equation and of the propagator, the method can be applied to spinors with different spatial localizations for spin-up and spin-down particles. In particular, it can be applied repeatedly for arbitrary times in spin separating dynamics without further modifications.

We choose the wave packets to have a zero net momentum in x and in y. The effect of adding an initial momentum to the wave packet adds an overall velocity to the individual spin components. Since S_y is a constant of the motion in the

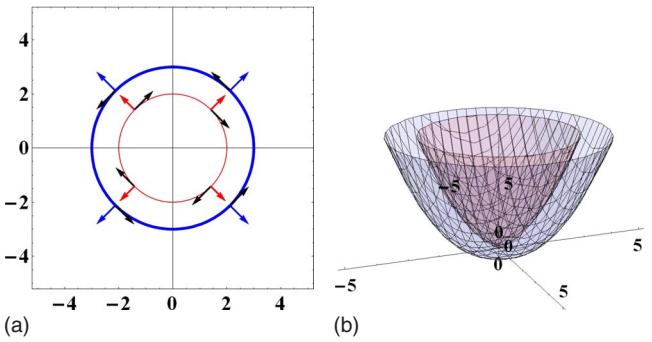

FIG. 1. (Color online) (a) The 2D electronic eigenstates for a Rashba SOC system in a momentum representation. The horizontal and the vertical axes are p_x and p_y, respectively. We label the net momentum with (radial) blue and red arrows and the eigenspinors with (azimuthal) black arrows. (b) The dispersion relation in the Rashba system. The colors of two parabola (blue and red) match the ones of two concentric circle in (a).

1D case, the dynamics is otherwise unaffected when plotting the y polarization. On the other hand, for the x and z polarizations, there will be additional features on top of a global translation in x, as is to be expected for a Rashba interaction defined in the rest frame of the material. These can be obtained following exactly the same procedure and we do not discuss them systematically in this paper. The absence of position dependence in the unconfined Rashba system implies that p_x and p_y are constants of the motion.

III. RESULTS

In this section we apply the propagator to localized wave packets in two situations: the 1D and the 2D Rashba systems. In each situation we consider both unconfined and confined cases. The eigenstates and eigenvalues for the Rashba system are provided in Fig. 1. In Fig. 1(a) two concentric circles correspond to two dispersion relations arising from the Rashba SOC for a fixed energy. Eigenspinors and momentum eigenvalues are given by azimuthal and radial arrows. In all cases, we consider the effect on the spin dynamics of changing two parameters: the Rashba coupling strength α and the width w of the initial wave packet. We provide plots with natural units $\hbar=1$, $m=1$. Note also that since we are interested in the influence of the width on the dynamics, we select an absolute length unit d such that the width w and the positions x and y are all expressed in terms of d rather than being correlated as a result of the choice of units. We also provide the units for the following variables: α in units of $\hbar^2/md$ and t in units of $md^2/\hbar$. This allows us to recover experimentally accessible values of the Rashba strength α by substituting realistic value of $\hbar$ and m and by choosing an appropriate length unit d. This also determines a unit width and a unit time and therefore realistic orders of magnitude for time and for wave packet width. In Sec. IV, we check this explicitly for an absolute length unit of 200 nm in 1D and verify that the corresponding Rashba strength is experimentally accessible. We then give an explicit quantitative description of how to find an appropriate value for d to match minimum and maximum experimentally accessible values of the Rashba strength in 2D.

We label spin states using the following convention: the up-in-x ($|\uparrow\rangle_x$) and down-in-x ($|\downarrow\rangle_x$) spin states correspond to a balanced superpositions of up-in-z ($|\uparrow\rangle$) and down-in-z ($|\downarrow\rangle$) spin states

$$|\uparrow\rangle_x = \frac{|\uparrow\rangle + |\downarrow\rangle}{\sqrt{2}}, \quad |\downarrow\rangle_x = \frac{|\uparrow\rangle - |\downarrow\rangle}{\sqrt{2}} \tag{10}$$

and similarly for up-in-y ($|\uparrow\rangle_y$) or down-in-y ($|\downarrow\rangle_y$) spin states

$$|\uparrow\rangle_y = \frac{|\uparrow\rangle + i|\downarrow\rangle}{\sqrt{2}}, \quad |\downarrow\rangle_y = \frac{|\uparrow\rangle - i|\downarrow\rangle}{\sqrt{2}}. \tag{11}$$

We plot the spin density $\langle \mathbf{S}\rangle(x,y)$ corresponding to the local expectation values of the spin operator.

A. One-dimensional Rashba system

Here we consider successively the unconfined and parabolically confined 1D Rashba system. For these 1D Rashba systems we select the x direction, corresponding to a horizontal line in Fig. 1(a), to make our analysis. The propagators used in this section are obtained in closed form as explained in Sec. II. An initial up-in-z spin state is chosen for all cases in the 1D Rashba system. We have observed four interesting features which we refer to as: spin separation (SS), bamboo-shooting structure (BSS), persistent spin helix structure (PSHS), and spin accumulation (SA). Note that SS, BSS, and PSHS are observed in the unconfined case and SA is observed in the confined case. We now discuss each of these features separately.

1. Spin separation

The Hamiltonian in Eq. (1) in the unconfined limit $\omega \to 0$ leads directly to two eigenspinors of S_y that travel with opposite velocities. On Fig. 1(a) this would correspond to red and blue arrows lying on the horizontal axis and pointing away from the center. When we add the opposite but unequal momentum contributions for a given spin in the inner and outer circles we see that spin up dominates on the right and spin down likewise on the left of the figure. This leads, for a localized wave packet, to a separation in x of two distinct y component of the spin as can be seen from the plot of $\langle S_y\rangle(x)$ in Fig. 2. We checked numerically that we can increase the rate of separation by increasing α.

Indeed, by increasing α we enlarge the difference between the two eigenenergies (the difference in radius of the circles). This in turn leads to a larger overall net momentum for each spin component and thus to a more rapid separation between the two spin components. The spreading of the wave packets depends both on α and w. The effect of w on the spreading is similar to that for the usual quantum spreading of free-particle wave packets: a small w leads to faster spreading. We notice that a smaller w also leads to faster spin separation as a result of the faster spreading. However the price to be paid is that the amplitude decreases as $\sqrt{1/(1+t^2/w^4)}$. As for α, we see slightly more spreading of the wave packet for

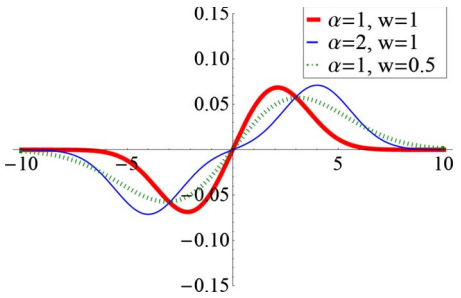

FIG. 2. (Color online) Spin density $\langle S_y\rangle(x)$ as a function of position x (in units of d) at $t=2$ (in units of $md^2/\hbar$) with different sets of α (in units of $\hbar^2/md$) and w (in units of d).

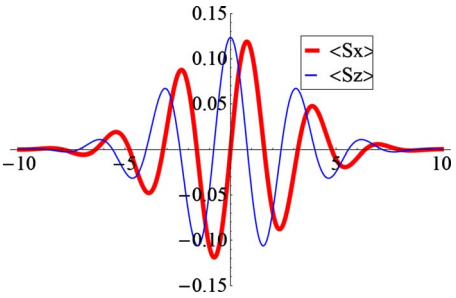

FIG. 4. (Color online) Spin densities $\langle S_x\rangle(x)$ and $\langle S_z\rangle(x)$ as a function of position x (in units of d) at $t=2$ (in units of $md^2/\hbar$), $w=0.5$ (in units of d), and $\alpha=1$ (in units of $\hbar^2/md$).

larger α. Related spin separation can be seen, for example, in the total densities ρ in 1D wave-packet dynamics study (See Ref. 26).

2. Bamboo-shooting structure

The BSS is observed in Fig. 3 for initial spins that are not eigenspinors of the Hamiltonian in Eq. (1) with $\omega\rightarrow 0$, such as the z component of the spin. Noneigenspinors can be expressed as superpositions of eigenspinors. Therefore an oscillation between the two eigenmodes arises. This has been referred to as a *Zitterbewegunglike* motion, an oscillatory motion between positive and negative energies as derived from Dirac's equation for relativistic electrons. Such intrinsic oscillations have been related to the occurrence of intersubband mixings[35] in contrast to the extrinsic oscillation which is caused by spin-dependent scattering.[36] The packet is extending in both directions at a constant velocity and oscillations extend (without moving) further at the same time. In this way a BSS, a successive "rise" of polarization at specific locations, is formed as the packet evolves.

As we increase α, we see fewer intrinsic oscillations: they occur only close to the original location of the wave packet. Indeed, a large α significantly decreases the overall amplitude of the oscillation. These oscillations can be related to the eigenspinors of the Hamiltonian traveling with opposite velocities. By measuring the noneigenspinors which are superpositions of eigenspinors, we find out that these eigenspinors tend to travel with opposite velocities. For relatively small α, the eigenspinors travel slower. Interference effects are more prominent for noneigenspinors due to the decreased propagation speed in opposite directions. As for the effect of w on intrinsic oscillations, we observe more intense oscillations for more localized packets.

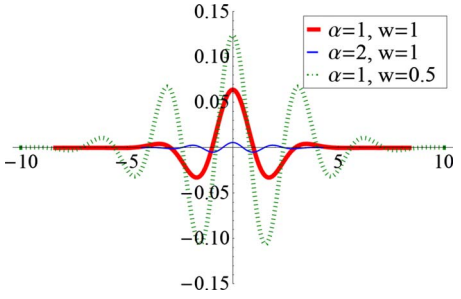

FIG. 3. (Color online) Spin density $\langle S_z\rangle(x)$ as a function of position x (in units of d) at $t=2$ (in units of $md^2/\hbar$) with different sets of α (in units of $\hbar^2/md$) and w (in units of d).

We also observe an attenuation in time of the BSS feature. To quantify the transient nature of the feature that we observe, we calculate the exponential decay of the center of the wave packet ($x=0$) and find

$$\langle S_z\rangle(0)=\frac{1}{\pi w^2}\sqrt{\frac{1}{1+\left(\frac{\hbar t}{mw^2}\right)^2}}\exp\left(-\frac{m^2t^2\alpha^2w^2}{m^2w^4\hbar^2+t^2\hbar^4}\right). \tag{12}$$

The contribution of the Rashba interaction (i.e., α-dependent factor) can be separated from the ordinary free-particle spreading. At short times we get a Rashba exponential attenuation proportional to $\exp(-\Gamma^2t^2)$, where $\Gamma=\frac{\alpha}{w\hbar}$. The value of the attenuation time Γ^{-1} is on the order of the picosecond, which is similar to the value found in the literature.[29] The attenuation times in Rashba systems are significantly longer than the Zitterbewegung decay times found in graphene and carbon nanotube work, as expected from the characteristic length scales involved.[30]

3. Persistent spin helix structure

By representing $\langle S_x\rangle(x)$ and $\langle S_z\rangle(x)$ on the same plot in Fig. 4, we see that the spin polarization correlates with the x position in what constitutes a spin helix. Since the packet is extending with a constant velocity in the x direction, its spin takes on the value given by $\langle S_x\rangle(x)$ and $\langle S_z\rangle(x)$ and therefore performs helicoidal motion as the packet spreads out. It is interesting to note that $\langle S_x\rangle(x)$ and $\langle S_z\rangle(x)$ are shifted in space with respect to each other. S_y corresponds to a conserved quantity leading to persistent behavior of the spin. This phenomenon has been predicted by Bernevig *et al.*[11] and has been recently observed by Koralek *et al.*[37] The period of the helix can be controlled by α: for bigger α the spatial period decreases. As in the case of the BSS, the PSHS disappears as a result of vanishing oscillations for increasing α. The persistent helix structure can be seen in other cases, such as the systems with combined Rashba and Dresselhaus effects balanced in strength. It has been shown that the combined system corresponds to a global spin rotation of a one-dimensional Rashba system.[11] We notice that having started

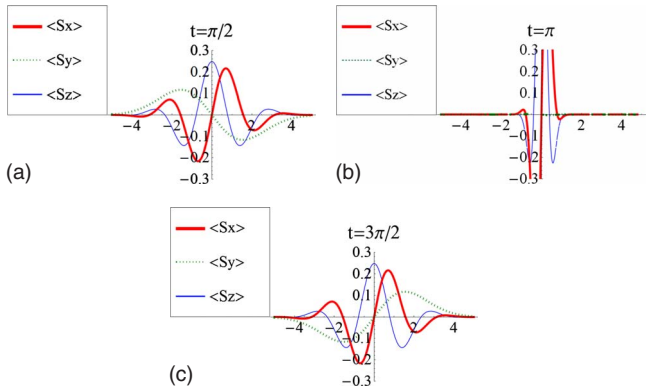

FIG. 5. (Color online) Spin densities $\langle S_x\rangle(x)$, $\langle S_y\rangle(x)$, and $\langle S_z\rangle(x)$ as a function of position x (in units of d) with $\alpha=1$ (in units of $\hbar^2/md$), $w=0.5$ (in units of d), and $\omega=1$ (in units of $\hbar/md^2$) evaluated at three different times (in units of $md^2/\hbar$).

from a localized Gaussian wave packet with finite width, the packet spreads as it moves and accordingly $\langle S_x\rangle(x)$ and $\langle S_z\rangle(x)$ decrease away from $x=0$. This feature is not to be attributed to a lack of persistence of the correlation between the spin orientation and the x position but to a decrease in the wave packet for larger distances. The spin helix is effectively transformed into a double Gaussian-shaped conical surface. In order to enhance the PSHS arising from the noneigenspinors, we have to reduce the spin-separation feature from the eigenspinors. This means that we can choose either a smaller α or a more localized wave packet, i.e., a smaller width w, to achieve the desired effect. The shift between the x and z polarizations has also been observed in time evolution of spin expectation values (See Ref. 13).

4. Spin accumulation

Confinement can cause specific spin components to accumulate at edges with either a hard wall potential or a harmonic-oscillator potential.[10] When we apply the confined propagator K^c_{1D} on the wave packet, we observe accumulations of specific spin components at the boundary in addition to the three features discussed above. Accumulation means that a given spin component appears at the boundary without oscillating from left to right.

We find two kinds of spin accumulation mechanisms: same spin components and opposite spin components at the boundary. Figure 5 exhibits the spin dynamics under the influence of a confining potential with an initial up-in-z spin state. We observe that for the eigenspinors, $\langle S_y\rangle(x)$ oscillates from left to right like a simple harmonic oscillator. For the noneigenspinors, we see that the z component oscillates with a reflection symmetry (even symmetry) around the $x=0$ and the same z component accumulating at the edge. In contrast, the x component oscillates without a reflection symmetry (odd symmetry) along the center line, leading to opposite spin components accumulating at the boundary. Note that the spin accumulation is only obtained for relatively small w. A possible reason is found in the faster spreading that follows from higher localization for fixed confining strength. The effect is also enhanced for small α due to the increase in the oscillations.

B. Two-dimensional Rashba system

We now proceed to analyze the wave-packet dynamics in the two-dimensional Rashba system. We consider both confined and unconfined systems. We use Trotter's formula from Sec. II to find the propagators. We obtain the evolution using Monte Carlo integration in Eq. (9).

Note that none of the three operators S_x, S_y, and S_z have global eigenspinors in momentum space in the 2D Rashba system. It is straightforward to show that the eigenspinors are momentum dependent, a fact which can also be seen in Fig. 1(a). In 1D Rashba systems, we confined the momentum distribution to be on either the x or the y axis leading to specific joint global eigenspinors of either the Hamiltonian and S_y or the Hamiltonian and S_x. In two-dimensional cases, such global eigenspinors do not exist. If the initial spin comes with a fixed momentum corresponding to a plane wave in a free-particle approximation, the eigenspinors can be identified from Fig. 1. Our task is to provide the Rashba dynamics of a Gaussian wave packet in coordinate space. The coordinate wave packet covers different sets of momentum-dependent eigenspinors as seen in Fig. 1(a) and therefore, the 2D oscillation originating from the superpositions in 2D Rashba systems has a more intricate structure. We observe four interesting features for four sets of initial spin states and measurements of the specific spin densities: ripple formation structure (RFS), triangular oscillations (TO), asymmetric spin rotations (ASR), and diagonal symmetry structure (DSS). We consider successively the effect of varying the Rashba coupling strength α, and the widths w_x and w_y of the initial Gaussian wave packet as we discuss these features.

1. Ripple formation structure

RFS is observed when the initial spin state is up-in z and the spin density $\langle S_z\rangle(x,y)$ is measured after a time t. As can be seen in Fig. 6, the wave packet exhibits peaks and troughs corresponding to regions of up-in-z and down-in-z spins.

We observe the effect of increasing the Rashba strength by comparing Figs. 6(a) and 6(b). The density of ripples increases with α and the up-in-z spin travels radially out. By increasing the width equally in two dimensions, we see fewer ripples for a fixed region of space when comparing Figs. 6(a) and 6(e). This is similar to the 1D case where multiple oscillations occur for highly localized wave packets. By changing the ratio of w_x and w_y we see that we can make the ripples less prominent in one direction or the other, as seen in Figs. 6(c) and 6(d).

We observe symmetry patterns in Fig. 6 which we now proceed to discuss. Within our numerical accuracy, we obtain azimuthal symmetry for the symmetric initial wave packets in Figs. 6(a) and 6(b). For unequal initial wave-packet localization in Figs. 6(c) and 6(d), we observe that the two figures are connected by a $\pi/2$ rotation relating the direction of enhanced fringes.

We notice that the direction along which the successive fringes appear are not purely horizontal [Fig. 6(c)] or vertical [Fig. 6(d)]. This effect can be understood from a semiclassical argument which indicates that a spin and momentum-dependent force induces a distortion. By working out the

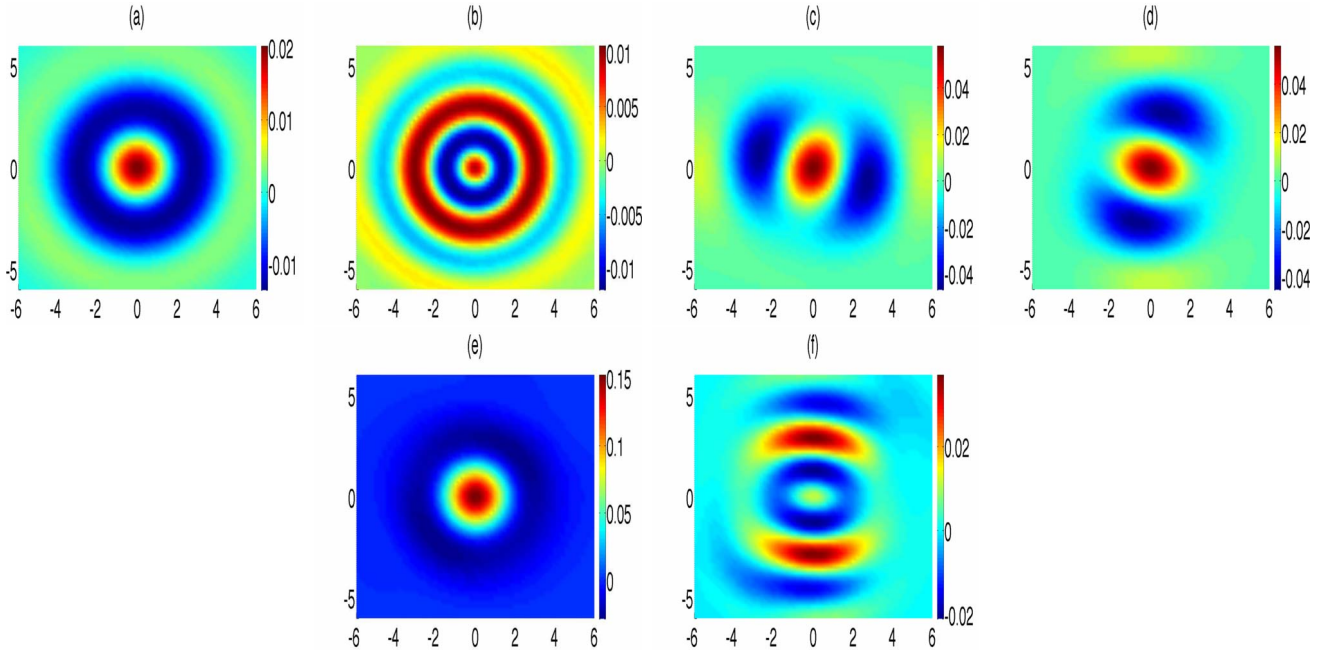

FIG. 6. (Color online) Spin-density $\langle S_z\rangle(x,y)$ contour plots for an initial up-in-z spin state evaluated at $t=3$ (in units of $md^2/\hbar$) with different α (in units of $\hbar^2/md$), w_x, and w_y (in units of d). (a) $\alpha=0.5$, $w_x=w_y=1.0$, (b) $\alpha=1.0$, $w_x=w_y=1.0$, (c) $\alpha=0.5$, $w_x=1.0$, $w_y=2.0$, (d) $\alpha=0.5$, $w_x=2.0$, $w_y=1.0$, (e) $\alpha=0.5$, $w_x=2.0$, $w_y=2.0$, and (f) $\alpha=1.0$, $w_x=2.0$, $w_y=1.0$.

Heisenberg equations of motion for the unconfined Rashba Hamiltonian, we obtain

$$\dot{p}_x = 0, \quad \dot{p}_y = 0, \quad \dot{x} = \frac{p_x}{m} - \frac{\alpha\sigma_y}{\hbar}, \quad \dot{y} = \frac{p_y}{m} + \frac{\alpha\sigma_x}{\hbar},$$

$$\dot{\sigma}_x = -\frac{2\alpha p_x \sigma_z}{\hbar^2}, \quad \dot{\sigma}_y = -\frac{2\alpha p_y \sigma_z}{\hbar^2},$$

$$\dot{\sigma}_z = \frac{2\alpha p_x \sigma_x}{\hbar^2} + \frac{2\alpha p_y \sigma_y}{\hbar^2}. \tag{13}$$

By considering the semiclassical force in the x direction, one shows that

$$F_x = m\ddot{x} = -\frac{m\alpha\dot{\sigma}_y}{\hbar} = \frac{2m\alpha^2 p_y \sigma_z}{\hbar^3} \tag{14}$$

and thus the force is both p_y and σ_z dependent, corresponding to the result of Fig. 6(d). This resembles a spin-dependent Coriolis force. As we observe from the figure, the upper and the lower half planes feel equal and opposite forces which leads to the distortion (since the wave packet itself is dispersing in two opposite y direction). A similar argument can be made using the vertical force F_y for Fig. 6(c). We note that the spin σ_z in Eq. (14) can be found for initial spin polarization along z to be $\sigma_z(t) = \sigma_z(0)\cos(2\alpha t\sqrt{p_x^2+p_y^2}/\hbar^2)$ so that the α dependence of the Coriolis force is not simply proportional to the strength of the Rashba coupling strength.

By comparing Figs. 6(d) and 6(f), we see again that a larger α causes the number of fringes to increase. The larger α value leads to the up-in-z spin traveling further from its initial central location in analogy to what we described in Fig. 6(b).

Recall that in the 1D Rashba system, the superposition of the two eigenstates represents an oscillation in space. Similarly in the 2D case, S_z does not have a global eigenspinor of the system, therefore it exhibits BSS in two dimensions with equal weights from x and y leading to circular ripple formation. The ripples appear for both large and small α, however, the crest of the ripple changes. For small α, the crest of the $\langle S_z\rangle(x,y)$ stays at the center with the wave propagating out similar to the BSS structure in 1D. As for large α, similarly to the case in 1D where noneigenspinors travel in opposite directions, $\langle S_z\rangle(x,y)$ travels out as a circular wave with a decreased amplitude. This can also be seen in the 1D BSS where smaller oscillations occur for larger α. Both eigenspinors of S_z travel with two larger group velocities. It should also be noted that more ripples appear in a fixed region of space for a larger α. This is consistent with the BSS discussed in Sec. III A 2. Circular ripples in 2D have been predicted for Gaussian wave-packet evolution.[26]

2. Triangular oscillations

Starting with an initial up-in-x spin state and measuring the spin density $\langle S_x\rangle(x,y)$, we observe TO from the contour plots in Fig. 7. By analogy with our discussion in 1D we know that the up-in-x spin state has a downward momentum when a y-localized wave packet is considered. The inclusion of x localization complicates the dynamics. There are two effects governing the dynamics: fringe formation in the x

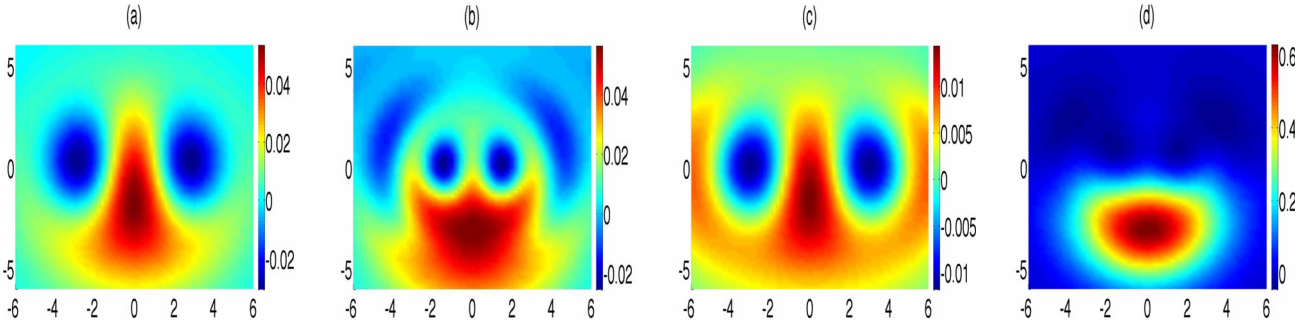

FIG. 7. (Color online) Spin-density $\langle S_x\rangle(x,y)$ contour plots for a initial up-in-x spin state evaluated at $t=3$ (in units of $md^2/\hbar$) with different α (in units of $\hbar^2/md$), w_x, and w_y (in units of d). (a) $\alpha=0.5$, $w_x=w_y=1.0$, (b) $\alpha=1.0$, $w_x=w_y=1.0$, (c) $\alpha=0.5$, $w_x=0.5$, $w_y=1.0$, and (d) $\alpha=1.0$, $w_x=2.0$, $w_y=2.0$.

direction and uniform downward (toward negative y) motion of the up-in-x wave packet.

In Fig. 7(a), it is clear that the spin is flipped on the horizontal axis on either side of the original location. This is a result of fringe formation as in the BSS in the 1D Rashba system. In Fig. 7(b), we see more fringes forming when we enlarge α. A larger α also leads to more downward momentum for the up-in-x spin. It is interesting to note that it is the part of the wave packet localized closest to the y axis that is moving downward. We observe the effect of even widths in Fig. 7(c), where we have a wave packet highly localized in x. By comparing Fig. 7(a) with Fig. 7(c) (α fixed), we see more fringes forming in the x direction. Figure 7(d) illustrates the fact that when we have a larger α and overall less-localized wave packets, again we see fewer fringes than in Fig. 7(b). In Fig. 7(d) the wave packet has moved further downward than in Fig. 7(c) due to a larger α which is consistent with previous observations and a faster downward momentum for the up-in-x component, which is consistent with all the observations in this feature.

The interplay between fringe formation and uniform downward motion leads to various dynamics. The larger α is, the more fringes (shorter wavelength) will form in the x direction, which is consistent with 1D BSS. At the same time, a larger α will lead to more momentum for the eigenspinors, which allows up-in x to move faster downward along the y axis. With a fixed α, the fringes can be enhanced (or suppressed) by selecting appropriate widths for the wave packet. In the case considered, where the fringes are formed only in the x direction, we need more (less) localization in x (y). The same applies in the y direction. This feature can also be observed if starting with a down-in-x spin. This choice leads to the vertical flipping of the result shown in Fig. 7. It should also be noted that this feature can be extended to the case where we have an initial spin state up-in y and we measure the $\langle S_y\rangle(x,y)$. The result would correspond to a $\pi/2$ rotation of the graphs shown in Fig. 7.

3. Asymmetric spin rotation

Starting with an initial up-in-z spin state and measuring the in-plane spin density $\langle S_x\rangle(x,y)$ or $\langle S_y\rangle(x,y)$, we observe an ASR in the contour plots of Fig. 8. Since an up-in-z spin state can be written as a superposition of either in x or y in spin space, measuring the dynamics of either x or y creates an interesting phenomenon. ASR is a rotation that should not be associated with the usual rotation in the x-y plane. By measuring the x component, we first immediately observe the two components separating in y. This separation is similar to the 1D localization case. The presence of the other dimension pulls the spin toward the other direction. As a result, the two opposite spin components start to perform ASR. ASR is a manifestation of the existence of a spin torque.[38]

It is straightforward to show that the rotation operator L_z is not a conserved quantity in the 2D unconfined Rashba system described by the Hamiltonian in Eq. (4) with $\omega=0$. Instead L_z+S_z is a conserved quantity in the system. It is also interesting to note that by providing an initial up-in-z spin state, we see a counterclockwise ASR while a clockwise ASR is observed for an initial down-in-z spin state. Again, there are two competing dynamical effects in this case: one is the fringe formation and the other is the motion of the eigenspinors. The fringe formation for the eigenspinors of S_x appears on the horizontal axis. The motion of the two eigenspinors is upward and downward, respectively, as can be seen in Fig. 1(a).

In Figs. 8(a) and 8(b), we see the effect of increasing α for a highly localized wave packet. Again, a larger α leads to a larger momentum for the two eigenspinors of S_x. A larger α also leads to more fringes as discussed in the previous two features. Therefore with the combination of these two effects for a larger α, we see a "banana cluster" forming up and down in Fig. 8(b). We show the effect of uneven widths in Fig. 8(c), where the high localization in x leads to more fringes in the x direction. By comparing Figs. 8(c) and 8(d), we see that the effect of increasing α leads to even higher fringe concentration. In Fig. 8(e), the fringes become less prominent as the wave packet is less localized. By comparing Figs. 8(e) and 8(f) we see that stronger upward and downward motion inhibits ASR. Finally we note that this feature of the spin density $\langle S_x\rangle(x,y)$ can also be observed for the spin density $\langle S_y\rangle(x,y)$ as a result of the symmetry of the Hamiltonian in Eq. (4) when $\omega=0$.

4. Diagonal symmetry structure

DSS is observed with an initial (x or y) in-plane spin state and a measurement of the other (y or x) in-plane components.

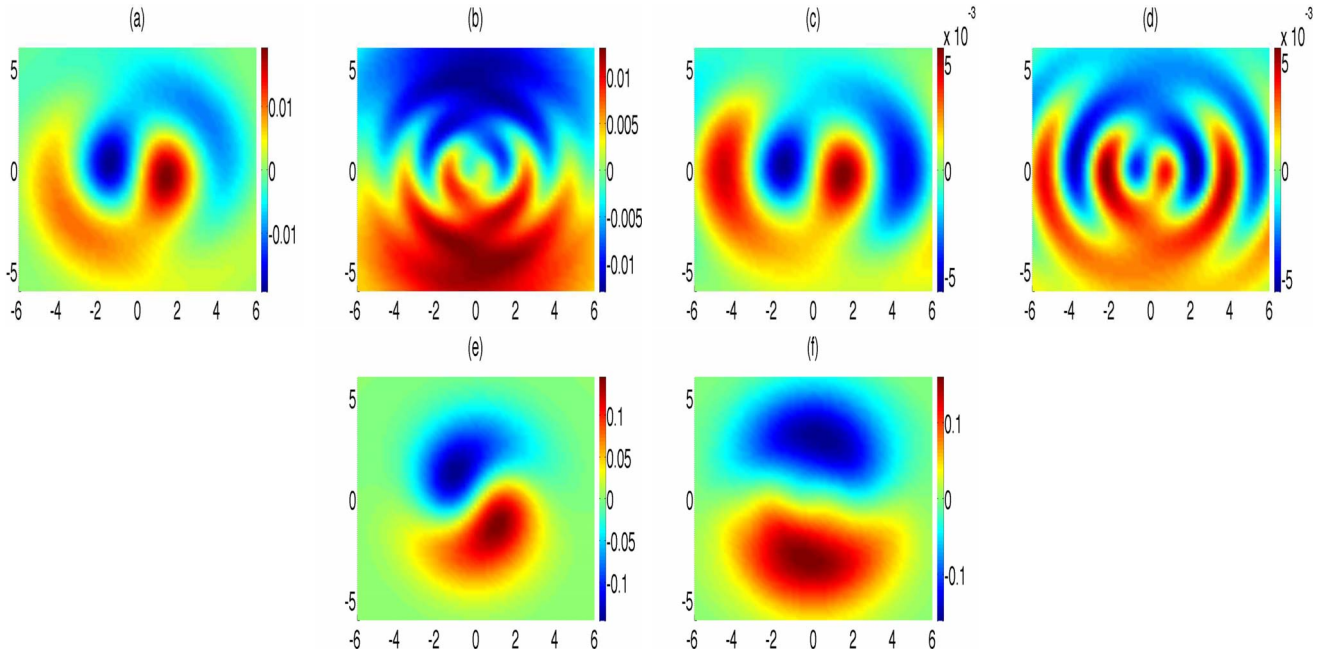

FIG. 8. (Color online) Spin-density $\langle S_x\rangle(x,y)$ contour plot for an initial up-in-z spin state evaluated at $t=3$ (in units of $md^2/\hbar$) with different α (in units of $\hbar^2/md$), w_x, and w_y (in units of d). (a) $\alpha=0.5$, $w_x=w_y=1.0$, (b) $\alpha=1.5$, $w_x=w_y=1.0$, (c) $\alpha=0.5$, $w_x=0.5$, $w_y=1.0$, (d) $\alpha=1.0$, $w_x=0.5$, $w_y=1.0$, (e) $\alpha=0.5$, $w_x=w_y=2.0$, and (f) $\alpha=1.0$, $w_x=w_y=2.0$.

For small α, we see two opposite y components of the spin moving downward and separating in the x direction. In the upper half of Fig. 9(a) the spin projection is reversed but less pronounced. This resembles a "four-leaf clover" structure. The up-in-y domain is along the main diagonal ($x=-y$) and the down-in-y domain is along the other diagonal ($x=y$). Although not perfect, the symmetry in Fig. 9 is based on the diagonals. The reflection symmetry does not exist about the x axis but about the two diagonal $x=y$ and $x=-y$ axes instead, corresponding to the traveling direction of two opposite spin components for larger α in Fig. 9(d).

As for the effect of localization, we see fewer fringes along the two diagonal lines for larger overall width of the wave packet. When changing the ratio of the horizontal and vertical widths, the effect is less significant than what we observed in other cases. This follows from the fact that the width does not correspond to the orientation of the fringes. By comparing Figs. 9(c) and 9(d), we see that the up-in-y and down-in-y components travel on the diagonal axes due to the combined effects of downward motion contributed from initial spin (up-in x) and of horizontal motion contributed from the measurement for the eigenspinors of S_y as can be checked in Fig. 1(a).

Lastly, we consider a 2D Rashba system with inclusion of a confining harmonic-oscillator potential in the x direction, as an illustration of the use of propagators in 2D confined systems. We see that the x confinement distorts the initially symmetric wave packets in Fig. 10(a) compared to the unconfined packet in Fig. 6(a). The unequal width in x and y still leads to additional ripples in Fig. 10(b) in analogy to Fig. 6(d) but now the confinement limits the spread of the wave packet in the x direction.

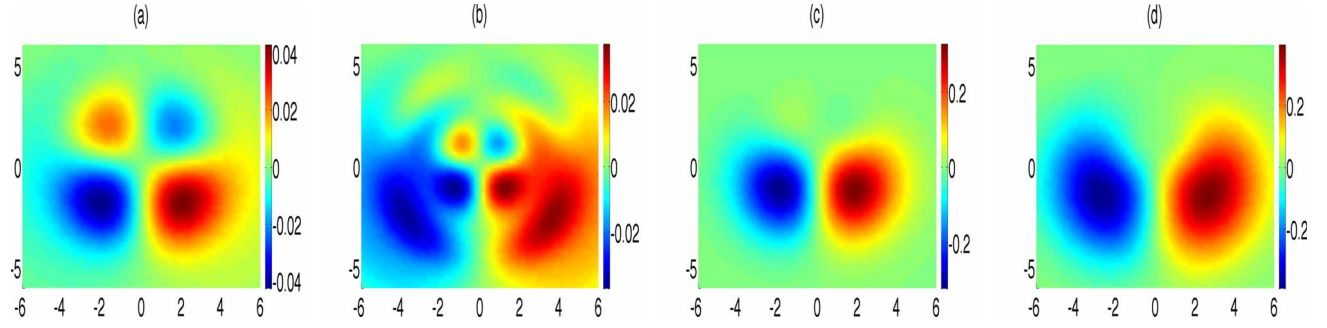

FIG. 9. (Color online) Spin-density $\langle S_y\rangle(x,y)$ contour plot for an initial up-in-x spin state evaluated at $t=3$ (in units of $md^2/\hbar$) with different α (in units of $\hbar^2/md$), w_x, and w_y (in units of d). (a) $\alpha=0.5$, $w_x=w_y=1.0$, (b) $\alpha=1.0$, $w_x=w_y=1.0$, (c) $\alpha=0.5$, $w_x=2.0$, $w_y=2.0$, and (d) $\alpha=1.0$, $w_x=2.0$, $w_y=2.0$.

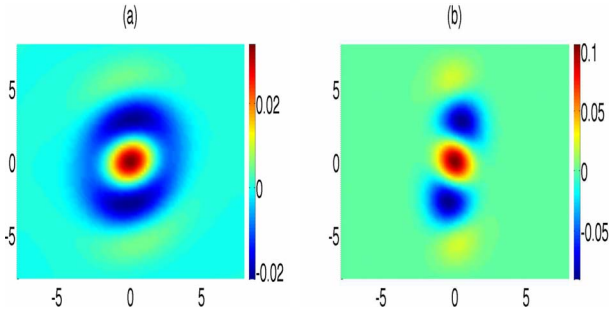

FIG. 10. (Color online) Spin-density $\langle S_z \rangle(x,y)$ contour plot for a initial up-in-z spin state evaluated at $t=3.0$. (a) $\alpha=0.5$, $\omega=0.5$, $w_x=w_y=1.0$ and (b) $\alpha=0.5$, $\omega=0.5$, $w_x=2.0$, $w_y=1.0$.

IV. DISCUSSION

We have plotted the spin densities $\langle S_x \rangle$, $\langle S_y \rangle$, and $\langle S_z \rangle$ for evolved Gaussian wave packets with different widths and initial spin states using the Rashba propagators with or without harmonic confinement and with different values of Rashba coupling strength α. In general, the plots show localized wave packets which have undergone spin-dependent separation, deformation, and spreading. They indicate where in space specific values of the spin operator components can be expected. The plots thus give a direct picture of polarization density.

All figures in this work are presented in scaled units which can be converted to realistic values that can be used to compare with experimental data. This can be achieved either by selecting an appropriate unit length d in the 1D case or by fitting d to recover specific values of α in the 2D case, with particular interest in recovering experimentally accessible values.

For example, in the 1D case, if we take the effective mass $m=0.05m_e$ (Ref. 26) and an absolute length unit $d=200$ nm, we can obtain a unit value of $\alpha=7.645\times10^{-12}$ eV m (bold and dotted lines in Figs. 2–5) two units of α, 1.529×10^{-11} eV m (thin line in Figs. 2 and 3) and a unit of time equal to $t=17.2$ ps. These values of α lie in the range of experimentally accessible Rashba strengths.[1] This choice also corresponds to wave packet widths $w=200$ nm (bold and thin lines in Figs. 2 and 3) or $w=100$ nm (dotted lines in Figs. 2–5), which are also in agreement with values found in the literature.[29] Using these values we obtain identical plots to those presented in Figs. 2–5 but now with realistic position values and expectation values on the axes.

The scaling in the 2D figures proceeds as follows. For example, in order to fit the minimum experimentally accessible α which is currently about 6×10^{-12} eV m to the scaled choice of $\alpha=0.5$ (low end), one selects the absolute length unit $d=127.43$ nm and the unit time $t=7$ ps. Similarly, one can fit $\alpha=1$ (high end) to the maximum experimentally accessible α which is currently about 4×10^{-11} eV m and again one can calculate the absolute unit length $d=38.23$ nm and the time unit $t=0.63$ ps.

All these results illustrate how the propagator allows us to track wave packets analytically, numerically, and pictorially for the study of Rashba systems. As might be expected, the Rashba interaction causes a spatial separation of the spin states: the twofold separation achieved in Fig. 2 is reminiscent of the Stern-Gerlach separation in an inhomogeneous magnetic field. More complex spatial patterns of polarization develop as a result of spreading, precession, geometry (2D), and confinement. As the wave packet spreads from its initial location as a result of the Rashba effect and as the electron precesses, the polarization will display an oscillation in space. Because the rates of spreading and precession are determined by the parameters, the maxima and the minima of the oscillation are fixed in space as in the PSHS seen in Fig. 4. When α increases, the velocity of separation increases also. However, if α is too large, the BSS feature is suppressed. On the other hand when α is too small, the Rashba effect is negligible and we recover free-particle behavior. Therefore, α should be carefully chosen depending on the specific purpose. For example, in the 1D case, for fixed width, spin separation will be enhanced by increasing the Rashba strength to $\alpha=1.529\times10^{-11}$ eV m, or beyond, using the maximum experimentally accessible value of $\alpha=4\times10^{-11}$ eV m.

When we increase the overall width w of the initial wave packet and therefore decrease localization, the wave packet spreads more slowly in analogy to free-particle spreading and we observe fewer fringes from the oscillations. Similarly, faster spreading occurs for smaller w. For example, for the experimentally accessible values of α, spin separation in Fig. 2 will be maximized by choosing a minimal width such as 100 nm in the 1D case and likewise for the 2D case. We also observe that the effect of the relative widths w_x/w_y on the fringe pattern depends on the particular spin components considered. For cases where initial polarization and measurement axis are given by, respectively (z and z), (x and x), and (z and x) in Figs. 6–8, the relative width plays an important role in the formation of fringes. This effect is suppressed when the initial and measured axes refer to orthogonal in-plane components (x and y) or (y and x). Again the optimal value of w_x and w_y should be selected for maximal effect.

We observe spatial separation and oscillations of the spin states in the 1D and 2D Rashba systems. The spatial separation of the spin states generates a *spin* current. This mechanism is enhanced by selecting a larger α, a smaller w, or both. On the other hand, the oscillations of the spin states is enhanced by selecting a smaller α, a smaller w, or preferably both. The system we considered is sufficiently complex that several of the features we identify occur simultaneously and are thus not necessarily mutually exclusive. Also the features we discuss arise in plots of different physical quantities. For example, the spin separation in Sec. III A 1 is observed in the y component in spin space whereas the BSS in Sec. III A 2 is observed at the same time and with comparable parameters but in the z component in spin space. The spin field-effect transistor proposed by Datta and Das[2] is an example of the use of an oscillation mechanism to control the spin. Some of the features described in this paper do appear in other work, although descriptions may vary. In particular SS, the components of BSS, the geometry of RFS, and the shifted components in PSH have previously been identified.[13,26]

We have presented a straightforward and flexible method to evaluate the spin dynamics in Rashba systems that can be extended to other SOC systems, such as Dresselhaus systems or a combination of the Rashba and Dresselhaus interactions. We have focused on the study of initial wave packets localized in position in 1D and 2D, unconfined and confined Rashba systems. The plots presented here are just a few selected examples of wave-packet evolution from which the main features were identified. These features do occur for values of the Rashba strength, wave-packet widths, and times which lie within the range of currently accessible values. The strength of the method can be shown effectively with the use of real-time animations. In conclusion this nonexhaustive study of wave-packet spin dynamics illustrates how propagator methods make it possible to retrieve complex information in SOC systems involving incompatible observables.

*bhsu@byu.net
†vanhuele@byu.edu

[1] D. Awschalom, *Semiconductor Spintronics and Quantum Computation*, 1st ed. (Springer, Berlin, 2002).
[2] S. Datta and B. Das, Appl. Phys. Lett. **56**, 665 (1990).
[3] I. Žutić, J. Fabian, and S. D. Sarma, Rev. Mod. Phys. **76**, 323 (2004).
[4] Supriyo Bandyopadhyay and Marc Cahay, *Introduction to Spintronics*, 1st ed. (CRC, Boca Raton, 2008).
[5] R. Winkler, *Spin-Orbit Coupling Effects in Two-Dimensional Electron and Hole Systems* (Springer, Berlin, 2003).
[6] J. Sinova, D. Culcer, Q. Niu, N. A. Sinitsyn, T. Jungwirth, and A. H. MacDonald, Phys. Rev. Lett. **92**, 126603 (2004).
[7] S-Q Shen, Phys. Rev. B, **70**, 081311(R) (2004).
[8] Y. K. Kato, R. C. Myers, A. C. Gossard, and D. D. Awschalom, Science **306**, 1910 (2004).
[9] B. A. Bernevig and S.-C. Zhang, Phys. Rev. Lett. **96**, 106802 (2006).
[10] X. Fu, W. Liao, and G. Zhou, Adv. Condens. Matter Phys. **2008**, 152731.
[11] B. A. Bernevig, J. Orenstein, and S. C. Zhang, Phys. Rev. Lett. **97**, 236601 (2006).
[12] M. H. Liu, K. W. Chen, S. H. Chen, and C. R. Chang, Phys. Rev. B **74**, 235322 (2006).
[13] J. Schliemann, D. Loss, and R. M. Westervelt, Phys. Rev. B **73**, 085323 (2006).
[14] P. Brusheim and H. Q. Xu, Phys. Rev. B **74**, 205307 (2006).
[15] E. I. Rashba, Fiz. Tverd. Tela (Leningrad) **2**, 1224 (1960) [Sov. Phys. Solid State **2**, 1109 (1960)].
[16] Yu. A. Bychkov and E. I. Rashba, J. Phys. C **17**, 6039 (1984).
[17] G. Dresselhaus, Phys. Rev. **100**, 580 (1955).
[18] A. Sarkar and T. K. Bhattacharyya, J. Appl. Phys. **101**, 036108 (2007).
[19] A. Sarkar and T. K. Bhattacharyya, Appl. Phys. Lett. **90**, 173101 (2007).
[20] J. Chen, W. Chao, and Q. W. Shi, Proceedings of the 2004 11th IEEE International Conference on Electronics, Circuits, and Systems, 2004, pp. 195–198.
[21] M. Pletyukhov and A. Shnirman, Phys. Rev. B **79**, 033303 (2009).
[22] A. Csordás, J. Cserti, A. Pályi, and U. Zülicke, Eur. Phys. J. B **54**, 189 (2006).
[23] Y.-Y. Chin, J.-Y. Chiu, M.-C. Chang, and C.-Y. Mou, J. Magn. Magn. Mater. **310**, e702 (2007).
[24] J. Brüning, V. Geyler, and K. Pankrashkin, J. Phys. A **40**, F697 (2007).
[25] J. Wang and C. Q. Wu, Chin. Phys. Lett. **25**, 3001 (2008).
[26] V. Ya. Demikhovskii, G. M. Maksimova, and E. V. Frolova, Phys. Rev. B **78**, 115401 (2008).
[27] K. Bencheikh and G. Vignale, Phys. Rev. B **77**, 155315 (2008).
[28] J. A. Lock, Am. J. Phys. **47**, 797 (1979).
[29] J. Schliemann, Phys. Rev. B **75**, 045304 (2007).
[30] W. Zawadzki and T. M. Rusin, arXiv:0909.0463 (unpublished).
[31] E. Merzbacher, *Quantum Mechanics*, 3rd ed. (Wiley, New York, 1998).
[32] Q. Wang, J. Phys. A **20**, 5041 (1987).
[33] B. C. Hsu and J.-F. S. Van Huele, J. Phys. A: Math. Theor. **42**, 475304 (2009).
[34] H. De Raedt and B. De Raedt, Phys. Rev. A **28**, 3575 (1983).
[35] J. Wang, K. S. Chan, and D. Y. Xing, Phys. Rev. B **73**, 033316 (2006).
[36] J. E. Hirsch, Phys. Rev. Lett. **83**, 1834 (1999).
[37] J. D. Koralek, C. P. Weber, J. Orenstein, B. A. Bernevig, S.-C. Zhang, S. Mack, and D. D. Awschalom, Nature (London) **458**, 610 (2009).
[38] A. Manchon and S. Zhang, Phys. Rev. B **79**, 094422 (2009).